ResearchGate

See discussions, stats, and author profiles for this publication at: https://www.researchgate.net/publication/45659325

In situ μgISAXS: II. Thaumatin crystal growth kinetic

ARTICLE *in* BIOPHYSICAL JOURNAL · AUGUST 2010

Impact Factor: 3.97 · DOI: 10.1016/j.bpj.2010.03.068 · Source: PubMed

CITATIONS
18

READS
37

4 AUTHORS, INCLUDING:

Ronald Gebhardt
Technische Universität München
49 PUBLICATIONS **457** CITATIONS

SEE PROFILE

Available from: Ronald Gebhardt
Retrieved on: 12 January 2016

In Situ μGISAXS: II. Thaumatin Crystal Growth Kinetic

Ronald Gebhardt,[†] Eugenia Pechkova,[‡] Christian Riekel,[†] and Claudio Nicolini[‡*]
[†]European Synchrotron Radiation Facility, B.P. 220, F-38043 Grenoble Cedex, France; and [‡]Nanoworld Institute, Interuniversities Research and Didactic Service Center on BioOrganic Nanosciences and Nanotechnologies (CIRSDNNOB), and Foundation for Advanced Electronics and Biotechnologies (Fondazione EL.B.A.), Genoa, Italy

ABSTRACT The formation of thaumatin crystals by Langmuir-Blodgett (LB) film nanotemplates was studied by the hanging-drop technique in a flow-through cell by synchrotron radiation micrograzing-incidence small-angle x-ray scattering. The kinetics of crystallization was measured directly on the interface of the LB film crystallization nanotemplate. The evolution of the micrograzing-incidence small-angle x-ray scattering patterns suggests that the increase in intensity in the Yoneda region is due to protein incorporation into the LB film. The intensity variation suggests several steps, which were modeled by system dynamics based on first-order differential equations. The kinetic data can be described by two processes that take place on the LB film, a first, fast, process, attributed to the crystal growth and its detachment from the LB film, and a second, slower process, attributed to an unordered association and conversion of protein on the LB film.

INTRODUCTION

Protein crystals grown on nanotemplate surfaces have some interesting features, such as enhanced radiation resistance (1,2). The growth of lysozyme films on lysozyme crystal surfaces has been studied by atomic force microscopy (3), but microscopic details of the crystal growth process under standard crystal growth geometries, such as the hanging-drop technique, are largely unknown. Grazing-incidence x-ray scattering (GISAXS) is an advanced scattering technique that can be used to investigate large-scale structures in thin films (4,5), including biofilms (6,7). A combination of this technique with synchrotron radiation microbeams (μGISAXS) has been used for studying surface gradients (8) or confined surfaces (9). The potential for studying thin protein films by μGISAXS during nanotemplate-assisted crystallization experiments was recently demonstrated in an ex situ experiment (10). Ex situ data obtained using both cytochrome P450scc and lysozyme were extremely complex to interpret and needed to be studied in parallel with microscopy characterization, using either the classical method or the nanotemplate hanging-drop method (10,11). The aim of this work is to demonstrate the possibility of studying protein crystallization by the hanging-drop technique directly in an in situ μGISAXS experiment.

EXPERIMENT

Samples

Thaumatin from *Thaumatococcus daniellii* (T7638, molecular mass 22 kDa) was purchased from Sigma Aldrich (Milan, Italy). Thaumatin protein monolayers were deposited on glass slides by the Langmuir-Schaefer method (12), which permits to obtain a highly packed and ordered thaumatin monolayer with a surface density of ~9.69×10^{10} molecules/mm^2, corresponding to ~10.32 nm^2/molecule, which fits well with the molecule geometric features from the Protein Data Bank (code 3DZR) and from atomic force microscopy measurements of Langmuir-Schaefer film (13). The 100 μl of filtered (0.45-μm filter unit, Millipore, Carrigtwohill, Ireland) protein solution of concentration 1 mg /ml were spread onto the air-water interface of the Langmuir-Blodgett (LB) trough with a Hamilton syringe (Reno, NV). Distilled water purified with a Milli-Q system (18.2 MΩ cm; Millipore, Billerica, MA) was used as subphase. The protein monolayer was compressed immediately after spreading to a surface pressure of 20 mN/m. Transfer of the protein monolayer from the subphase surface onto a solid support was performed by touching the support parallel to the subphase surface according to the LS technique (horizontal lift) at a fixed surface pressure. The crystallization conditions used for the hanging-drop method here reported, with two LB layers of thaumatin, were as follows. A 4-μl drop containing 15 mg/ml of thaumatin in 100 mM ADA buffer, pH 6.5, was mixed with 4 μl of the reservoir solution (1 M sodium/potassium tartrate in 100 mM sodium/potassium tartrate buffer, pH 6.5) and placed on a siliconized glass slide in the classical method, or on a thaumatin nanotemplate in the LB method, and stabilized over the reservoir containing 1 M sodium/potassium tartrate in 100 mM sodium/potassium tartrate buffer, pH 6.5. For rapid buffer exchange, the reservoir was connected via teflon tubes with two Harvard syringe pumps (see Fig. 2 of the accompanying article (13)). The salt concentration in the reservoir, $m(t)$, was calculated according to

$$m(t) = V_0 \times \rho_1 + (m_0 - V_0 \times \rho_1) \times e^{-\frac{\frac{dV_1}{dt}}{V_0} \times t}.$$

Submitted August 11, 2009, and accepted for publication March 22, 2010.

*Correspondence: manuscript@ibf.unige.it

Ronald Gebhardt's present address is Institute for Food Process Engineering and Dairy Technology Weihenstephan, Technical University Munich, Weihenstephaner Berg 3, 85350 Freising, Germany.

Editor: Leemor Joshua-Tor.

© 2010 by the Biophysical Society

0006-3495/10/08/1262/6 $2.00

doi: 10.1016/j.bpj.2010.03.068

where m_0 is the initial amount of salt in the reservoir at time $t = 0$, V_0 the initial volume, dV_1/dt the incoming volume flux, and ρ_1 the density of salt. The absolute value of the outgoing flux is also dV_1/dt (see Fig. 2 of the accompanying article (13)).

Experimental layout

A modified hanging-drop crystallization cell was developed for in situ μGISAXS experiments, and for buffer exchange, the reservoir was connected via Teflon tubes to two Harvard syringe pumps (13). The conditions used for buffer exchange protocol during alignment and experiment preparation were as follows. In the drop, 7.5 mg/ml protein was mixed with 0.5 M Na/K tartrate in 100 mM ADA buffer, and the reservoir solution was 0.5 M Na/K tartrate in 50 mM ADA buffer. For experiment initiation, the reservoir solution was changed to 1 M Na/K tartrate in 100 mM ADA buffer.

Experiments were performed at the ID13 microfocus beamline at the European Synchrotron Radiation Facility in Grenoble, France (14). The monochromatic beam ($\lambda = 0.991$ Å) was focused by crossed Fresnel lenses (10) on a spot of dimensions $0.5 \times 1\ \mu m^2$ (full width at half-maximum) at the sample position (15) with ~10^{10} photons/s at 12.7 keV. The μGISAXS pattern was recorded by a MAR165 CCD detector (2000×2000 pixels with a 78.94×78.94-μm pixel size; 16-bit readout). The sample-to-detector distance was 791 mm, determined by an Ag-behenate standard (16).

A typical μGISAXS patterns is shown in our previous work (12). Specular scattering is observed for $Q_x = Q_y = 0, Q_z > 0$, and diffuse scattering for $Q_x, Q_y \neq 0$. Correlations vertical to the sample surface can be probed along Q_z at $Q_y = 0$. Characteristic morphological parameters, such as shape and distances of the sample, can be extracted by analysis of out-of-plan scans in the Q_y direction, as discussed in detail elsewhere (4). Critical angles of thaumatin and glass for the used x-ray energy were calculated on the basis of their chemical formula and densities. The Fit2D software package was used for data reduction (17). For further data analysis and generation of graphics, SigmaPlot (Systat Software, Chicago, IL) was used. Kinetic modeling was performed with isee systems (Stella, Fairport, NY) and Mathematica (Champaign, IL).

RESULTS AND DISCUSSION

Detector scans were created from the 2D GISAXS pattern by cutting along the Q_z axis at $Q_y = 0$. Fig. 1 *A* shows a projection of the temporal variation of the detector cuts. The direct beam at $\alpha_f = -0.71°$ and the specular beam at $\alpha_f = 0.71°$ are striking features and do not change in position with time. Both beams generate small-angle scattering. This scattering broadens the specular beam and causes scattered intensity between $\alpha_f = -0.2°$ to $-0.5°$ for the direct beam. Variation in intensity with time can be found in the angular range $\alpha_f = 0.1$–$0.6°$. These so-called intensity fringes increase after the first 50 min and finally drop after 400 min. They are a result of correlated surface roughness (18,19), i.e., correlated processes of thaumatin absorption on the LB film due to its surface morphology. Fig. 1 *B* illustrates the correction for the small-angle scattering contribution of the direct beam at the onset of the kinetics ($t = 0$ min) and at the end ($t = 972$ min). The scattering was modeled by fitting two Gaussian profiles around the direct beam. The obtained profiles were summed and used for the background correction.

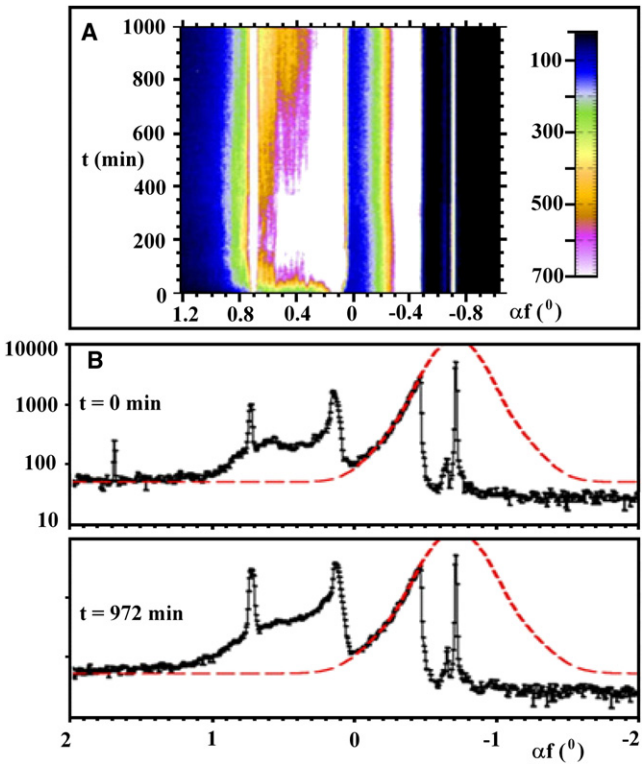

FIGURE 1 (*A*) Time dependence of the detector cuts (direct beam, $\alpha_f = -0.71°$; solution scattering, $\alpha_f = -0.2$ to $-0.5°$; Yoneda region, $\alpha_f = 0.1$–$0.6°$; specular beam, $\alpha_f = 0.71°$). (*B*) Background correction for the detector cuts at $t = 0$ and $t = 972$ min. Small-angle x-ray scattering around the direct beam ($\alpha_f = -0.71°$) is fitted by a set of two Gaussian profiles (*red curves*).

The Yoneda region (Fig. 2) of the background-corrected detector scans is shown selectively for $t = 0$, 400, and 972 min. The Yoneda peak consists of a contribution from glass ($\alpha_c = 0.14°$) and a contribution from protein ($\alpha_c = 0.11°$) (Fig. 2, *arrows*). Compared to the glass signal, the scattering contribution from the protein is weak. After 400 min, the maximum intensity of the overlapping protein/glass Yoneda peak is increased by one order of magnitude compared to the case at the beginning of the kinetics. After this, the intensity drops to approximately one-half of the value at the end of the measured kinetics ($t = 972$ min).

The temporal variation of the intensity ratio (protein/glass) is shown in Fig. 3 *A*. The ratio was calculated by relating the intensity value at $\alpha_f = 0.11°$ to the intensity value at $\alpha_f = 0.14°$. In general, the plot shows that the proportion of the

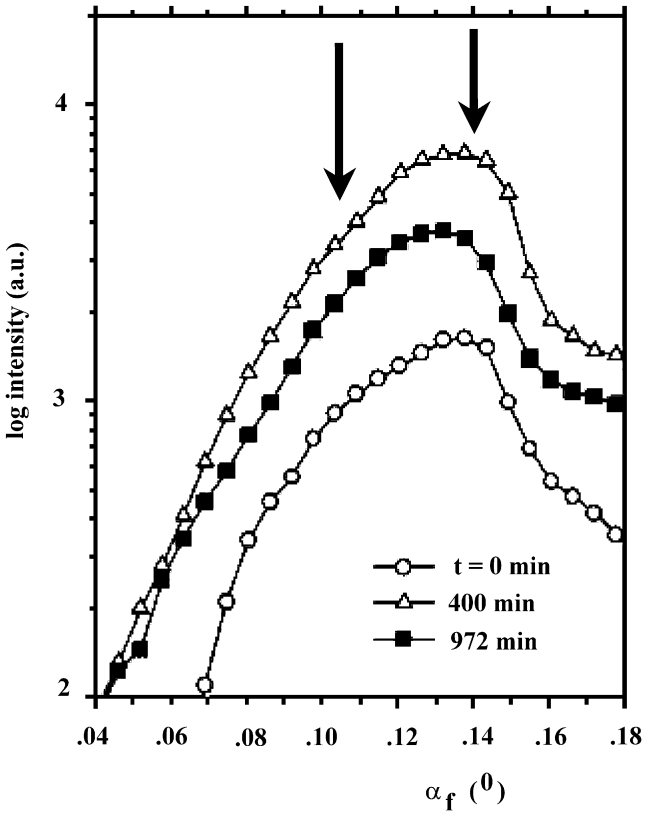

FIGURE 2 Background corrected Yoneda peak at $t = 0$ min (*open circles*), $t = 400$ min (*open triangles*), and $t = 972$ min (*solid squares*) consisting of a constant substrate contribution (Si/SiO_2 at $\alpha_f = 0.14°$) and a variable protein contribution (thaumatin at $\alpha_f = 0.11°$).

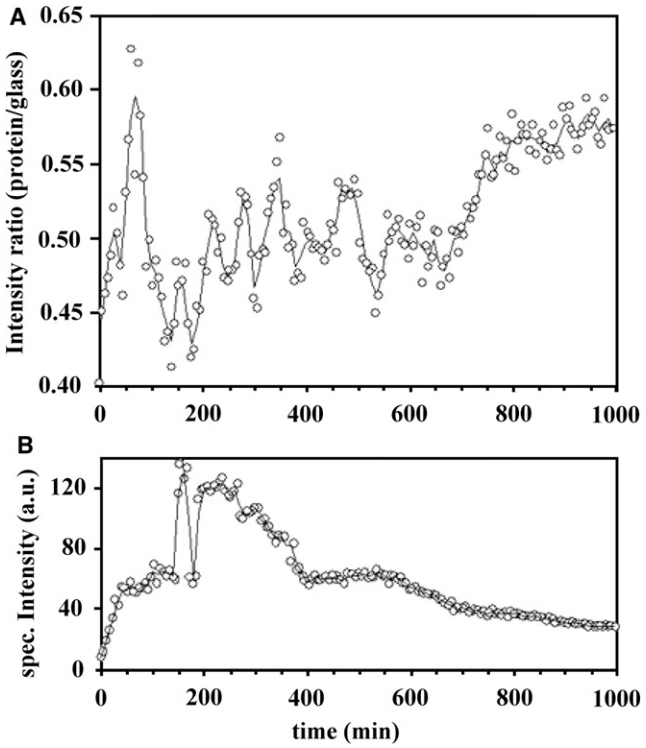

FIGURE 3 (*A*) Variation of the intensity ratio of protein ($\alpha_f = 0.11°$) to glass ($\alpha_f = 0.14°$). (*B*) Variation of specular intensity with time.

protein attached to glass increases. In more detail, a fast steep increase and decrease of the ratio appears within the first 200 min. After this, the protein/glass ratio increases more or less monotonously. In the case of the Yoneda peak of glass, we can assume an invariance with time. Actually, as shown in Fig. 2, both intensity values, at $\alpha_f = 0.11°$ and $\alpha_f = 0.14°$, vary with time. This means that the peak height of the Yoneda peak of glass is affected by changes of the protein Yoneda peak. For this reason, we deal in absolute values in the following discussion. Changes in the Yoneda region can be referred to the interplay between specular and diffuse scattering. Fig. 3 *B* shows the variation of the specular intensity with time. It is obvious that the specular intensity increases considerably between $t = 100$–300 min. This means that the film roughness decreases in this period.

In the beginning of the kinetic, the GISAXS experiment is conducted on the thaumatin-LB film. The LB film contains two layers of thaumatin molecules. Lateral spatial correlations of the film lead to a contribution of diffuse scattering to the overall GISAXS scattering distribution and can be studied by means of Q_y cuts. Fig. 4 *A* displays the temporal evolution of Q_y cuts taken from the two-dimensional GISAXS pattern at the critical angle of the protein ($\alpha_c = 0.11°$). The smooth decay in intensity of the cuts with increasing Q_y can be well approximated by two Gaussian profiles. When comparing the cuts, a peak at $Q_y = 0.1$ nm^{-1} measured after $t = 100$ min becomes conspicuous. Such a feature in the Q_y cut indicates highly ordered crystalline regions in the LB film and was analyzed in more detail (Fig. 4 *B*). The data were fitted by a model that assumes structures arranged in a bidimensional paracrystal (20,21). The model fit provided a mean distance between adjacent structures on the LB film of $D = 58$ nm. We assign this distance to the spacing between adjacent crystalline seeds that are on the verge of being secreted from the thaumatin nanotemplate into the reservoir. Under the assumption that the Yoneda peak of glass does not change during the association processes, we evaluated the temporal change of the intensity on the critical angle of the protein ($\alpha_c = 0.11°$). The kinetics of the thaumatin μGISAXS pattern was measured at different positions on the LB film. The absolute temporal variation of the thaumatin Yoneda peak intensities is shown in Fig. 5.

Each curve in Fig. 5 shows a steep increase in the intensity in the first 50 min. At $t = 180$ min the signals reach a first maximum. The intensities increase again after 200 min and reach a second intensity maximum after ~450 min. Finally, the intensities drop. The averaged data (*heavy line*) shows the same time evolution as the individual curves. The averaged curve was analyzed with system dynamic models to specify the temporal processes. The simplest model able to describe the kinetic curves of Fig. 5 is shown schematically

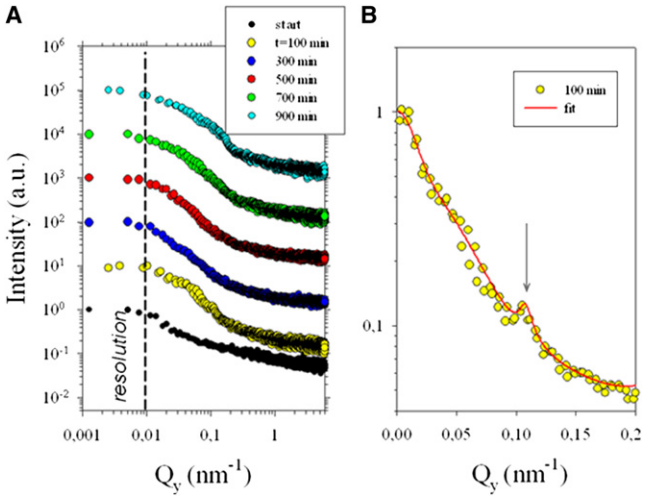

FIGURE 4 (*A*) Double logarithmic plot of horizontal (Q_y) line cuts taken from the two-dimensional GISAXS signal at different times. The calculated experimental resolution in the Q_y direction is shown as a vertical dashed line. (*B*) Cut at $t = 100$ min for a more restricted Q-range showing a peak at $Q_y = 0.1$ nm^{-1}.

in Fig. 6. The corresponding model curve, together with the temporal processes of the basic components is shown in Fig. 7. The mathematical formalism is described in the Appendix. The model assumes a reservoir of an oversaturated protein solution, P_1, which corresponds to the thaumatin in the hanging drop. The change of the reservoir concentration results from a process that leads to a protein association on the LB film. The association depends on the amount of protein in the reservoir, P_1, on the amounts of the LB film states, P_2 and P_3, and association rates k_1 and k_3, respectively. The temporal change of the amount of protein P_1 is shown as a dotted line in Fig. 7. Its association leads to the association states P_{12} and P_{13} of the LB film.

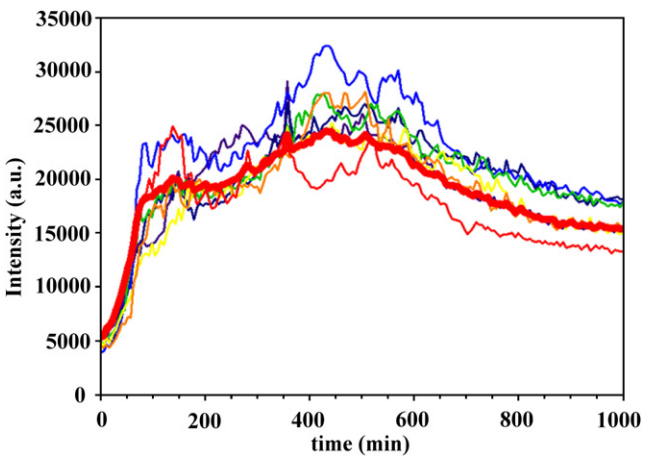

FIGURE 5 Variation of the intensity at the protein Yoneda peak as a function of time. Single measurements are represented by thin lines and the average by the heavy line.

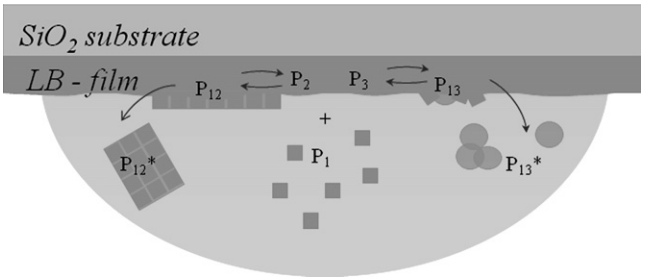

FIGURE 6 Model for association pathways on LB film (see text).

Besides the protein inflows, the concentration of the associated states depends also on their rates of conversion (k_2 and k_4) into the end states P_{12}* and P_{13}*. Both conversions lead to a decrease of protein in the LB film due to dissociation reactions. The change of the associated state P_{12} (see Fig. 7, *black solid line*) corresponds to the thaumatin crystalline state in the LB film, which leads to increased specular intensity due to a smoother surface (compare Fig. 3 *B*) and a crystalline structure factor peak in the Q_y cut (compare Fig. 4 *B*). Its fast formation and dissociation takes place at high thaumatin concentration in the reservoir (Fig. 7, *dotted line*). Moreover, the formation of P_{12} starts from the intensity level of the LB film, which acts as a seed for crystal growth. After reaching the maximum at $t = \sim$100 min, the process drops down to zero, which means that the crystalline state becomes completely depopulated in favor of the crystalline state P_{12}*. This state corresponds to a completely dissociated crystal, leaving a hole in the LB film. The formation of associated state P_{13} runs more slowly (Fig. 7, *dashed line*). In contrast to the temporal change of P_{12}, this process first starts at zero and in a second stage proceeds at comparatively low thaumatin concentrations in the hanging-drop reservoir. The former means that the state P_{13} is not populated at the

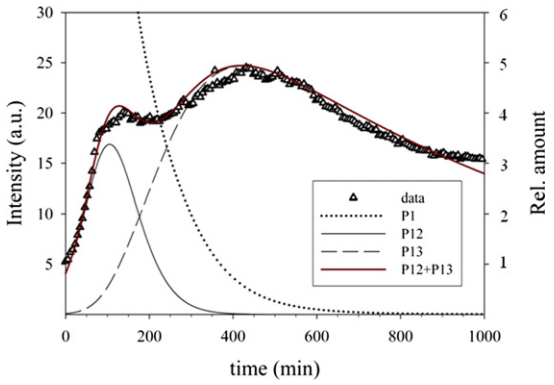

FIGURE 7 Analysis (*red line*) of the averaged protein kinetic data (*triangles*) according to the system dynamic approach scheme. A relative amount of 1 corresponds to a thaumatin monolayer. The fit results from the arbitrary scaling of the sum of the amounts of thaumatin in the template-associated states P_{12} and P_{13}. Both association states modify the originally smooth double-layered template's thickness and roughness and are therefore a good measure of the resulting GISAXS signal.

beginning and not comparable to the ordered thaumatin state in the LB film. Hence, we identify this state as a less ordered thaumatin protein that associates at low free thaumatin concentrations on the LB film. The degradation of the less ordered state at $t > 500$ min can have different causes. Normal protein degradation or an onset of LB film disruption due to the long duration of the experiment at room temperature (295 K) and the radiation damage have to be taken into consideration.

It is obvious that these experiments must be pursued, in particular as the glass scattering has to be quantitatively subtracted in the future from the protein signal. The glass scattering is unfortunately quite strong. However, this is always the case in first experiments. The write-up is largely based on the model of the crystallization process.

APPENDIX

Modeling of protein association

The reaction equations (Eqs. 1 and 2) correspond to the reaction pathways schematized in Fig. 6.

$$\begin{aligned} &P_1 + P_2 \underset{k_1}{\overset{k_{-1}}{\leftrightarrow}} P_1P_2,\\ &P_1 + P_1P_2 \leftrightarrow (P_1)_2P_2,\\ &P_1 + (P_1)_{n-1}P_2 \leftrightarrow (P_1)_nP_2,\\ &(P_1)_nP_2 \underset{k_2}{\rightarrow} (P_1)_nP_2^* \end{aligned} \tag{A1}$$

$$\begin{aligned} &P_1 + P_3 \underset{k_3}{\overset{k_{-3}}{\leftrightarrow}} P_1P_3,\\ &P_1 + P_1P_3 \leftrightarrow (P_1)_2P_3,\\ &P_1 + (P_1)_{m-1}P_3 \leftrightarrow (P_1)_mP_3,\\ &(P_1)_mP_3 \underset{k_4}{\rightarrow} (P_1)_mP_3^* \end{aligned} \tag{A2}$$

where P_1 is the thaumatin protein and P_2 and P_3 are two states of the LB film. $(P_1)_nP_2$ and $(P_1)_mP_3$ are corresponding association states with n and m bounded thaumatin molecules, respectively (referred to as P_{12} and P_{13} in Figs. 6 and 7) The association reactions are reversible and determined by the rates k_1, k_{-1}, k_3, and k_{-3}. The final states $(P_1)_nP_2$* and $(P_1)_mP_3$* are formed via an irreversible reaction with the rates k_2 and k_4 (P_{12}* and P_{13}* in Figs. 6 and 7) First-order differential equations were derived from the reactions. The equation system was solved by the Euler-Cauchy method.

$$\begin{aligned} \frac{dP_1}{dt} &= -k_1 \times P_1 \times P_2 - k_3 \times P_1 \times P_3 \\ &\quad + \{k_{-1} \times P_1P_2 + k_{-3} \times P_1P_3\}\\ \frac{dP_1P_2}{dt} &= k_1 \times P_1 \times P_2 - k_2 \times P_1P_2 - \{k_{-1} \times P_1P_2\}\\ \frac{dP_1P_2^*}{dt} &= k_2 \times P_1P_2\\ \frac{dP_1P_3}{dt} &= k_3 \times P_1 \times P_3 - k_4 \times P_1P_3 - \{k_{-3} \times P_1P_3\}\\ \frac{dP_1P_3^*}{dt} &= k_4 \times P_1P_3. \end{aligned} \tag{A3}$$

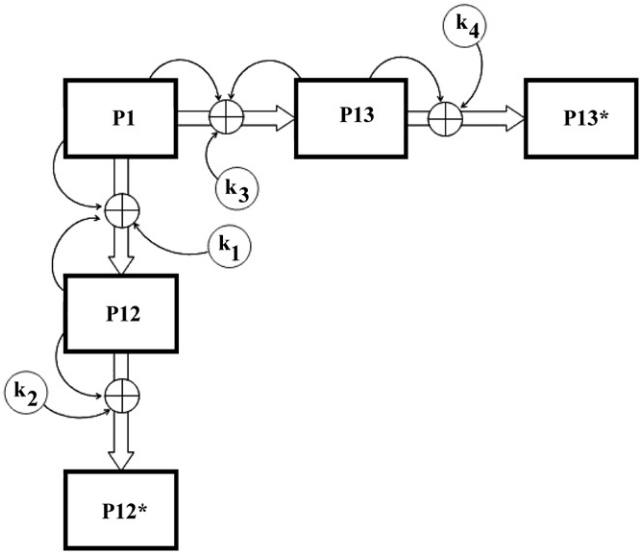

FIGURE 8 Flow-chart of the association model.

For simplicity, two assumptions were made: 1), the n and m bidirectional association reactions were replaced by one unidirectional association reaction; and 2), the LB state P_2 in the differential equations (Eq. A3) was replaced by the association states P_1P_2, since both states consist of a high number of thaumatin molecules and differ by only one molecule – the same was done with LB state P_3. The flow-chart diagram (Fig. 8) illustrates the model assumptions.

The authors thank Manfred Burghammer for setting up the beamline and Peter Müller-Buschbaum for stimulating discussions, and we declare no conflicts of interest.

This project was supported by grants to Fondazione El.B.A. by the Ministero dell'Istruzione, dell'Università e della Ricerca (MIUR) for "Funzionamento" and for Biocatalysis Programma Nazionale di Ricerca and by a Fondo per gli Investimenti della Ricerca di Base International Grant on Proteomics and Cell Cycle (RBIN04RXHS) from MIUR to Interuniversities Research and Didactic Service Center on BioOrganic Nanosciences and Nanotechnologies, Nanoworld Institute of the University of Genoa. R.G. acknowledges funding of his position through the FP6 SAXIER grant.

REFERENCES

1. Pechkova, E., and C. Nicolini. 2003. Proteomics and Nanocrystallography. Kluwer Academic Press, Dordrecht, The Netherlands.
2. Pechkova, E., G. Tropriano, …, C. Nicolini. 2004. Radiation stability of protein crystals grown by nanostructured templates: synchrotron microfocus analysis. *Spectrochim. Acta B. At. Spectrosc.* 59:1687–1693.
3. Li, H. Y. A., A. Nadarajah, and M. L. Pusey. 1999. Determining the molecular-growth mechanisms of protein crystal faces by atomic force microscopy. *Acta Crystallogr. D Biol. Crystallogr.* 55:1036–1045.
4. Müller-Buschbaum, P., S. V. Roth, …, C. Riekel. 2003. Multiple-scaled polymer surfaces investigated with micro-focus grazing-incidence small-angle x-ray scattering. *Europhys. Lett.* 61:639–645.
5. Rauscher, M., T. Salditt, and H. Spohn. 1995. Small-angle x-ray scattering under grazing incidence: the cross section in the distorted-wave Born approximation. *Phys. Rev. B.* 52:16855–16863.
6. Müller-Buschbaum, P., R. Gebhardt, …, W. Doster. 2007. Effect of calcium concentration on the structure of casein micelles in thin films. *Biophys. J.* 93:960–968.

7. Spaar, A., C. Münster, and T. Salditt. 2004. Conformation of peptides in lipid membranes studied by x-ray grazing incidence scattering. *Biophys. J.* 87:396–407.

8. Roth, S. V., M. Burghammer, …, H. Walter. 2003. Self-assembled gradient nanoparticle-polymer multilayers investigated by an advanced characterisation method: microbeam grazing incidence x-ray scattering. *Appl. Phys. Lett.* 82:1935–1937.

9. Roth, S. V., T. Autherieth, …, P. Mueller-Buschbaum. 2007. In situ observation of nanoparticle ordering at the air-water-substrate boundary in colloidal solutions using x-ray nanobeams. *Appl. Phys. Lett.* 91:091915.

10. Nicolini, C., and E. Pechkova. 2006. Structure and growth of ultrasmall protein microcrystals by synchrotron radiation: I microGISAXS and microdiffraction of P450scc. *J. Cell. Biochem.* 57:544–552.

11. Pechkova, E., and C. Nicolini. 2006. Structure and growth of ultrasmall protein microcrystals by synchrotron radiation: II. microGISAX and microscopy of lysozyme. *J. Cell. Biochem.* 97:553–560.

12. Nicolini, C., and E. Pechkova. 2006. Nanostructured biofilms and biocrystals. *J. Nanosci. Nanotechnol.* 6:2209–2236.

13. Pechkova, E., R. Gebhardt, …, C. Nicolini. 2010. In situ μGISAXS I: Experimental set up for submicron study of protein nucleation and growth. *Biophys. J.* In press.

14. Riekel, C., M. Burghammer, …, D. Popov. 2009. Fundamentals of noncrystalline diffraction with microfocus techniques. *In* Applications of Synchrotron Light to Non-Crystalline Diffraction in Materials and Life Sciences. M. García-Gutiérrez, A. Nogales, M. Gómez, and T. A. Ezquerra, editors. Lecture Notes in Physics, Vol. 776, Springer, Heidelberg, Germany.

15. Noehammer, B., C. David, …, C. Riekel. 2005. Coherence-matched microfocusing of hard x-rays. *Appl. Phys. Lett.* 86:163104.

16. Blanton, T. N., T. C. Huang, …, T. Raftery. 1995. JCPDS-International Centre for Diffraction Data round robin study of silver behenate. A possible low-angle x-ray diffraction calibration standard. *Powder Diffr.* 10:91–95.

17. Hammersley, A. 2009. The FIT2D Home Page. www.esrf.fr/computing/scientific/FIT2D/. ESRF, Grenoble, France.

18. Holy, V., and T. Baumbach. 1994. Nonspecular x-ray reflection from rough multilayers. *Phys. Rev. B.* 49:10668–10676.

19. Pechkova, E., S. V. Roth, …, C. Nicolini. 2005. μGISAXS and protein nanotemplate crystallization: methods and instrumentation. *J. Synchrotron Rad.* 12:713–716.

20. Lazzari, R. 2002. IsGISAXS: a program for grazing-incidence small-angle x-ray scattering analysis of supported islands. *J. Appl. Crystallogr.* 35:406–421.

21. Gebhardt, R., C. Vendrely, …, C. Riekel. 2009. Characterization of the boundary zone of a cast protein drop: fibroin β-sheet and nanofibril formation. *Langmuir.* 25:6307–6311.